Check for updates

Geophysical Research Letters

RESEARCH LETTER
10.1029/2022GL101838

Key Points:

- Eight-year seismic data scrutinized by template matching provide ~4 times more events before the M_w 6.0 Amatrice mainshock
- Fore-mainshocks and swarm-like clusters persisted before the 2016 Amatrice mainshock at the northern and southern fault edges
- An unlocking process by progressive seismicity localization weakened the 2016 main fault volume peripheral area

Supporting Information:

Supporting Information may be found in the online version of this article.

Correspondence to:

M. Sugan,
msugan@ogs.it

Citation:

Sugan, M., Campanella, S., Chiaraluce, L., Michele, M., & Vuan, A. (2023). The unlocking process leading to the 2016 Central Italy seismic sequence. *Geophysical Research Letters*, *50*, e2022GL101838. https://doi.org/10.1029/2022GL101838

Received 21 OCT 2022
Accepted 12 JAN 2023

© 2023. The Authors.
This is an open access article under the terms of the Creative Commons Attribution-NonCommercial-NoDerivs License, which permits use and distribution in any medium, provided the original work is properly cited, the use is non-commercial and no modifications or adaptations are made.

The Unlocking Process Leading to the 2016 Central Italy Seismic Sequence

M. Sugan[1], S. Campanella[1], L. Chiaraluce[1,2], M. Michele[2], and A. Vuan[1,2]

[1]National Institute of Oceanography and Applied Geophysics—OGS (Italy), Trieste, Italy, [2]Istituto Nazionale di Geofisica e Vulcanologia (Italy), Rome, Italy

Abstract Approximately 23,000 well-located earthquakes from 2009 to 2016 are used as templates to recover seismic activity preceding the 2016 Central Italy seismic sequence. The resulting spatiotemporal pattern is analyzed by additional ~91,000 newly detected events. In the 8 years before the sequence onset, seismicity ($M_L \leq 3.7$) develops at the hangingwall of the 2016 normal faults and along a sub-horizontal shear zone, bounding the active extensional system at depth. This activity, mainly organized in foreshock-mainshock and swarm-like clusters, migrates toward the nucleation area of the first M_w 6.0 mainshock of the sequence (24th of August in Amatrice). We propose an unlocking process based on variable temporal clustering of the seismicity, including repeaters, identifying fault portions with different degrees of coupling. Such a progressive localization of the seismic activity at the fault edges induces a weakening of the locked patch of the Amatrice mainshock.

Plain Language Summary We exploit a high-resolution seismic catalog to describe the activity preceding the 2016 Central Italy sequence. Newly retrieved events are analyzed in space and time to characterize the earthquake preparatory phase leading to the first mainshock of the sequence. Our 8-year-long observations show that most seismic activity involves structures surrounding the nucleation and rupture zone. Interesting seismicity patterns are found along an almost horizontal discontinuity below the upper crustal normal faults and at their northern and southern edges. We highlight migrations, clustering, and progressive seismicity localization close to the first mainshock of the sequence, unveiling a complex preparatory phase.

1. Introduction

In the last 25 years, the central Apennines have been the site of moderate-strong ($5.9 \leq M_w <= 6.5$) extensional earthquakes (Colfiorito 1997; L'Aquila 2009; Central Italy 2016). Contrary to what happened in both 1997 (Ripepe et al., 2000) and 2009 (Lucente et al., 2010) crises, the 2016 sequence initiated without conventional foreshocks activity (e.g., Vuan et al., 2017).

The sequence evolved around its largest event (M_w 6.5, 30th October) near Norcia, located in the middle of a fault system activated 2 months earlier, with a first M_w 6.0 (24th August) event located south, near the town of Amatrice. Then, a few days before the Norcia earthquake, another M_w 5.9 event occurred at the northernmost extent of the sequence, near the village of Visso (Figure 1).

Aftershocks distribution shows the geometry of the shallow SW-dipping normal fault segments hosting the mainshocks of the sequence, confined at depth by a sub-horizontal, approximately 2–3 km thick, shear zone (SZ) active between 7 and 12 km (SZ; Chiaraluce et al., 2017; Waldhauser et al., 2021); a discontinuity interpreted as a litho-structural feature or as the limit of the brittle-ductile transition, contributing differently to pre- co- and post-seismic displacement (respectively Barchi et al., 2021 and Mandler et al., 2021).

Before the M_w 6.0 Amatrice mainshock, seismicity rate changes along the SZ (Vuan et al., 2017) and pre-slip (Vičič et al., 2020) linked to supposed temporal fluctuations in tectonic loading are observed close to the system of shallow dipping normal faults.

In the 8 months preceding the 2016 sequence onset, seismic activity increased along the SZ in the areas located at the termination of the normal faults that will host the strongest earthquakes. These time-varying rates have been interpreted as the brittle signature of the final stage of the tectonic loading process acting along the normal fault's bounding plane, suggesting an active role of the SZ in the preparatory earthquake phase (Vuan et al., 2017). On the contrary, Tan et al. (2021) and Waldhauser et al. (2021) observed that during the aftershock sequence,

19448007, 2023, 5, Downloaded from https://agupubs.onlinelibrary.wiley.com/doi/10.1029/2022GL101838 by CochraneItalia, Wiley Online Library on [24/03/2023]. See the Terms and Conditions (https://onlinelibrary.wiley.com/terms-and-conditions) on Wiley Online Library for rules of use; OA articles are governed by the applicable Creative Commons License

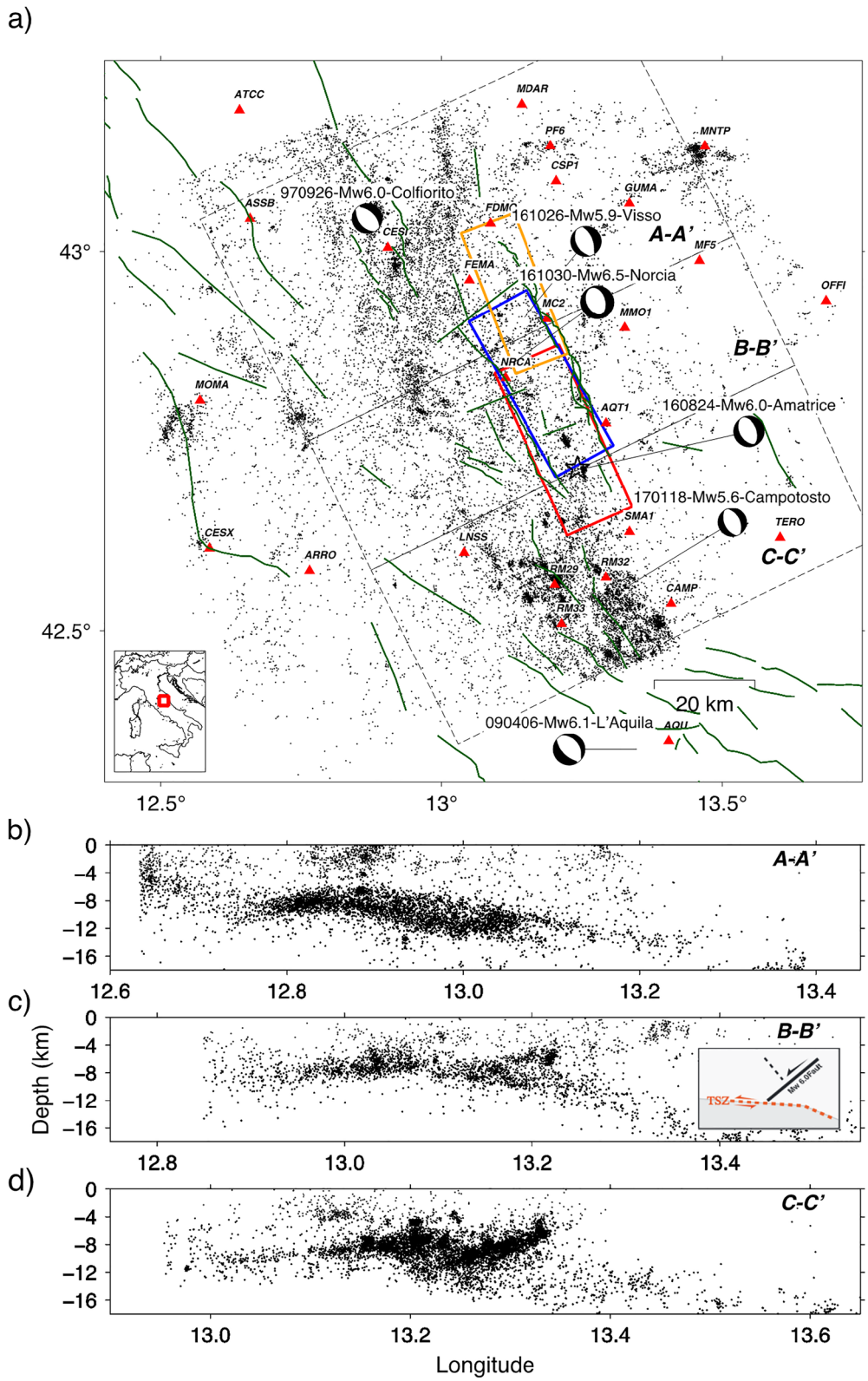

Figure 1.

19448007, 2023, 5, Downloaded from https://agupubs.onlinelibrary.wiley.com/doi/10.1029/2022GL101838 by CochraneItalia, Wiley Online Library on [24/03/2023]. See the Terms and Conditions (https://onlinelibrary.wiley.com/terms-and-conditions) on Wiley Online Library for rules of use; OA articles are governed by the applicable Creative Commons License

19448007, 2023, 5, Downloaded from https://agupubs.onlinelibrary.wiley.com/doi/10.1029/2022GL101838 by CochraneItalia, Wiley Online Library on [24/03/2023]. See the Terms and Conditions (https://onlinelibrary.wiley.com/terms-and-conditions) on Wiley Online Library for rules of use; OA articles are governed by the applicable Creative Commons License

seismicity along the SZ mainly occurs in response to the slip on the normal faults, proposing a passive role for this structure during the coseismic stage. All these findings suggest a time-dependent and evolving behavior for the SZ.

To investigate the driving process leading to the unlocking mechanisms of the 2016 seismic sequence and to better understand the role of the SZ and surrounding fault system, we increase the spatio-temporal resolution of the seismicity patterns, placed between Colfiorito 1997 and L'Aquila 2009 (Figure 1), over the 8 years before the sequence onset.

To look for previously undetected events, we first relocated the catalog of ∼23,000 earthquakes within the source volume of the 2016 Central Italy sequence. Seismic events were detected by the Italian National Network (ISIDe Working Group, 2007) from the 1st of January 2009 and the 24th of August 2016, the day of the Amatrice mainshock (Figure 1). This starting catalog is then used in a template matching framework (Gibbons & Ringdal, 2006; Sugan et al., 2014, 2019; Vuan et al., 2018, 2020) to generate an augmented catalog that we used to identify areas with different frictional properties looking at the occurrence over time and space of diverse typologies of clusters (e.g., foreshock-mainshock, mainshock-aftershock, or swarm-like; Zaliapin & Ben-Zion, 2016, 2020).

Within the events characterized by higher waveforms similarity, we look for repeating earthquakes to be possibly associated with the occurrence of aseismic slip, such as creeping, afterslip, or slow slip events (e.g., Uchida, 2019).

These features are then discussed with respect to models proposed for the earthquake preparation phase and nucleation process (Ellsworth & Bulut, 2018; Kato & Ben-Zion, 2021; Tape et al., 2018).

2. Methods

2.1. Input Catalog

The catalog of templates consists of 23,003 events in the local magnitude (M_L) range 0.1–5.2 that occurred in the 100 × 100 km^2 area shown in Figure 1 from the 1st of January 2009 to the onset of the 2016 Central Italy sequence (24th of August 2016). The events have been initially relocated in absolute terms using NonLinLoc code (Lomax et al., 2000), based on a nonlinear inversion method (Figures S1 and S2, in Supporting Information S1). Then, to further maximize the quality of the templates' catalog in terms of hypocentral location resolution, we apply a double difference (Waldhauser & Ellsworth, 2000) scheme, taking only absolute travel times. The resulting relocations show the mean value of horizontal errors of ∼500 m in an east-west direction and ∼400 m north-south (Figure S3 in Supporting Information S1). Details about the methods are described in supplement Text S1 in Supporting Information S1.

2.2. Template Matching

Template matching search for earthquakes that strongly resemble well-located events called templates. We apply the method developed by Vuan et al. (2018) to 8-year continuous data (Figure S4, in Supporting Information S1) to gain greater detail in microseismicity patterns. Text S2 in Supporting Information S1 describes input and output parameters to infer and validate the augmented catalog (Figure S5 in Supporting Information S1). We keep the new detections co-located with the templates, while the magnitude is estimated by amplitude comparison with the templates.

2.3. Clustering Analysis and Repeating Earthquakes

We analyze the clustering of the events in the augmented catalog over time and space (see Text S3 in Supporting Information S1 by applying the Zaliapin and Ben-Zion (2016, 2020) approach that separates the clusters from the background seismicity (Figure S6 in Supporting Information S1). Subsequently, following the criterion proposed by Ogata and Katsura (2012), we define and classify the clusters as swarms, mainshock-aftershock, and foreshock-mainshock sequences (Figure S7 and Text S3 in Supporting Information S1).

Figure 1. (a) Map showing the selected templates (black dots) and stations (red triangles) used in the template matching analysis. Faults are projected at the surface as boxes: Amatrice (red, Tinti et al., 2016), Visso (orange, Chiaraluce et al., 2017), Norcia (blue, Scognamiglio et al., 2018). The star marks the 24th August Amatrice epicenter. Green lines show normal faults (Barchi et al., 2021). Focal mechanisms from Scognamiglio et al., 2006. (b) A-A', (c) B-B', (d) C-C' along dip cross-sections of seismicity from 2009 to 2016 (24th August), where is apparent the almost flat shear zone (SZ) in the middle crust. In (c), a simplified scheme of the top of SZ (TSZ) and the normal fault.

19448007, 2023, 5, Downloaded from https://agupubs.onlinelibrary.wiley.com/doi/10.1029/2022GL101838 by CochraneItalia, Wiley Online Library on [24/03/2023]. See the Terms and Conditions (https://onlinelibrary.wiley.com/terms-and-conditions) on Wiley Online Library for rules of use; OA articles are governed by the applicable Creative Commons License

Then, to better define the fault properties, we investigate the temporal clustering in terms of the coefficient of variation of interevent times (Kagan & Jackson, 1991) and seismic moment ratio evolution over time (e.g., Cabrera et al., 2022). The first defines the level of temporal clustering as close to 0 for periodic seismicity and greater than 1 for temporally clustered sequences; the second provides indications when most of the seismic moment can be associated with a single event (values close to 1) or when no prevailing event is found (values relative to 0). We also explore the mechanical properties of the activated faults and surrounding regions by focusing on the presence of repeating earthquakes (Figure S8 in Supporting Information S1). In particular, we adopt a method that combines both seismic waveform similarity, using a cross-correlation function and differential S-P travel time measured at each seismic station (Sugan et al., 2022). Details about the parameters and the approach adopted to declare repeating earthquakes are provided in Supporting Information S1 (Text S4).

3. Results

In the 8-year preceding the Amatrice earthquake, template matching helped detect approximately 91,000 new events (*Catalog_TM* in Supporting Information S1), lowering the magnitude of completeness (M_C) of the augmented catalog by about 1 degree of magnitude, reaching $M_C = 0.4$ (Figures S9a and S9b in Supporting Information S1). The resulting catalog reflects the seismic data availability over time (Figure S4 in Supporting Information S1), including events with a high degree of waveform similarity (cross-correlation values >0.9; Figure S9c in Supporting Information S1).

The augmented catalog identifies microseismic activity in key sectors of the complex system of faults that have been activated during the sequence. Most seismicity is located below 7 km, while the 2016 main sequence spreads a broader range, including the shallower crustal volume (<7 km; Figure S10 in Supporting Information S1).

We analyze the pre-sequence augmented catalog by dividing the events according to their position above and below the SZ top (TSZ). By applying a tuned ridge estimator of the scattered seismicity (Amini & Roozbeh, 2015), we identify a smooth 3D surface at TSZ (Figure S11 in Supporting Information S1).

The TSZ east-dipping boundary is evident below and north of the 2016 fault system, while in the southern sector, it mixes up in terms of both seismic activity (e.g., aftershocks) and geometry with the deeper and low-angle portion of the Campotosto fault, activated with a series of $5 < M_W < 6$ events during the 2009 L'Aquila sequence (Valoroso et al., 2013). TSZ depth values range from 7 to 12 km and do not differ significantly from the TSZ reconstructed in Vuan et al. (2017).

A space and time representation of the 8-year augmented catalog and the corresponding yearly frequency of events are shown in Figure 2. Seismicity is projected along the 2016 main faults mean strike (336°–N24 W, Tinti et al., 2016) with positive and negative offset values, respectively, toward the north and south of the 24th of August Amatrice mainshock hypocenter. Figure 2 highlights two main features: (a) the migration in time of the shallower activity (above the TSZ) from Campotosto to the Amatrice region (Figures 2a and 2b) and (b) the lack of activity along the SZ right below the Amatrice fault (Figures 2c and 2d).

From 2009 to 2013, the clustering of events above the SZ migrates off-fault from Campotosto to the southernmost edge of the Amatrice fault, activating later the main fault volume (Figure 2b and Movie S1).

While remaining active during the 8-year time window, the SZ concentrates the events north and south of the Amatrice main fault edges (see Figures 2c and 2d, and Movie S2). Below this fault, a lower seismicity rate is found (Figure 2d).

The period from 2009 to the end of 2011 is characterized by a concentration of events in the Campotosto area (south of the 2016 main fault: Figure 2). We interpret this activity as part of the still ongoing aftershocks activity of the 2009 L'Aquila sequence, presumably extended in time due to the triggering effect of the pore pressure diffusion process, also described by Malagnini et al. (2012). Our new catalog confirms the migration process occurring in Campotosto and in a larger area than the one observed by Malagnini et al., 2012. However, the apparent diffusivity values ~50–70 m^2/s we retrieve using 2 years of seismic activity (Figure S12a in Supporting Information S1) are consistent with previous observations made by Malagnini et al. (2012), using only the first month of aftershocks. From 2009 to 2010 (Figure S12b in Supporting Information S1), we observed an average migration velocity of about 7 km/decade, pointing to the 2016 leading fault. After 2013, we still observe activity in the southern part of the Amatrice fault (Figures 2a and 2c), in the Campotosto area, even if the number

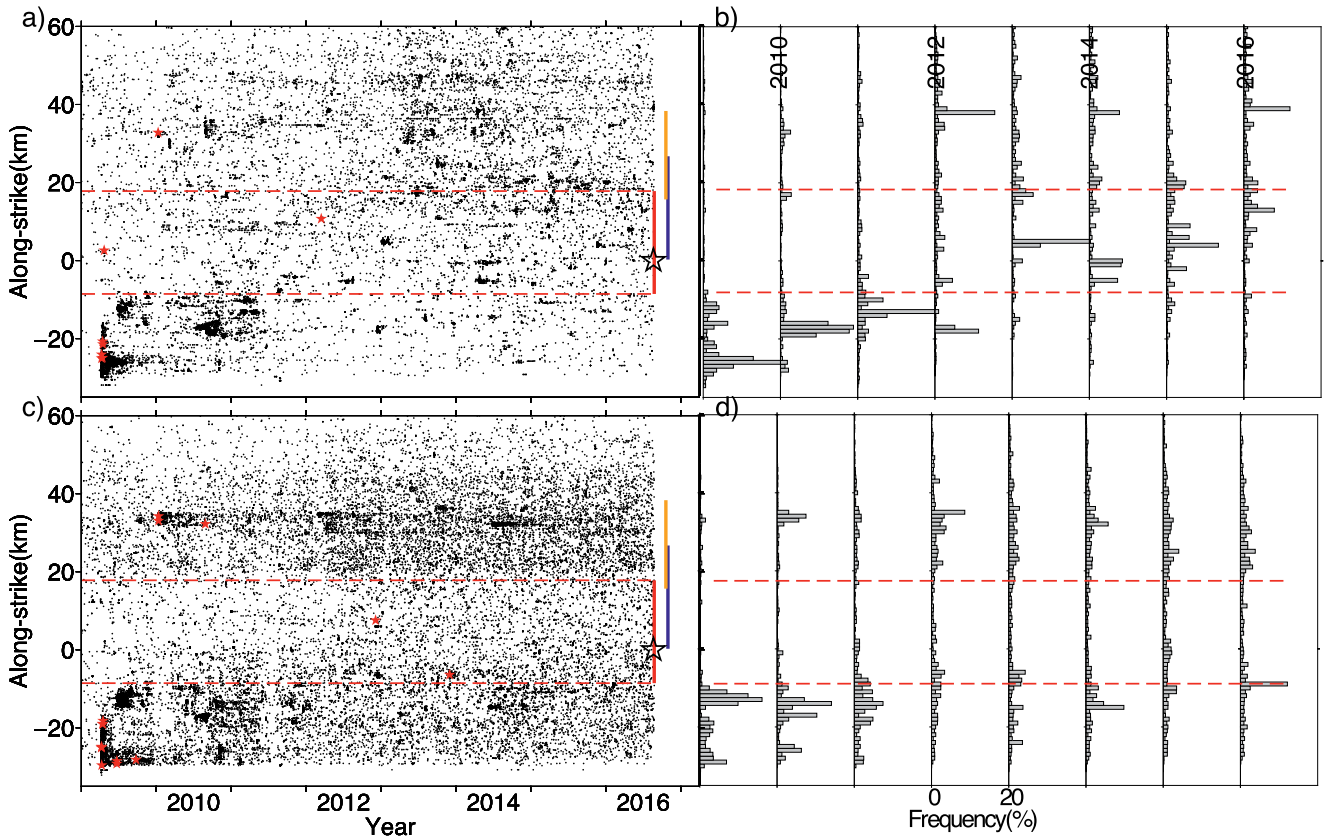

Figure 2. (a) Spatiotemporal distribution of the augmented catalog in the shallow crust above the TSZ and (b) the yearly frequency of events projected along the main fault strike (336°). Only events with $M \geq$ Mc are plotted. (c, d) panels as (a, b) for events below the TZS. Red dotted lines represent the northern and southern edges of the 24th August M_w 6.0 Amatrice main fault. Faults are projected at the surface for the Amatrice mainshock (red), Visso (orange), and Norcia (blue). The black stars mark the 24th August Amatrice epicenter as a reference, and the red stars mark $M > 3.5$ events.

of events decreases (Figures 2b and 2d). Inside the Amatrice fault volume, clusters above the TSZ have been observed starting from 2013 (Figures 2a and 2b). At the same time, sparse unclustered seismicity is active close to the northern fault edge within the SZ (Figures 2c and 2d). Movies S1–S3 to the supplement show the events' migration and the activation of different critical areas around the main fault area.

In the following, we apply a space-time nearest-neighbor technique (Zaliapin & Ben-Zion, 2016, 2020) to distinguish clustered from background activity (Figure 3), plus a frequency-magnitude distribution criterion (Ogata & Katsura, 2012) for classifying the identified clusters as swarm-like, foreshock-mainshock, and mainshock-aftershock.

Within our 8-year catalog, we identify approximately 670 clusters (with a number of events higher than 10) lasting from days to months and a maximum magnitude generally lower than M_L 3 (Figure S13 in Supporting Information S1). These clusters constitute almost 51% of the total seismicity and are mainly foreshock-mainshock (22%) or swarm-like sequences (28%); there are very few typical mainshock-aftershock.

Figures 3a and 3b help distinguish reference areas with clustered or unclustered distributed seismicity above and below TSZ. In the shallow crust (Figure 3a), clusters are mainly found in the hanging wall of the fault system (Movie S3) and predominate in the southern sector (S) or within the fault volume (F). Few clusters characterize the northern sector (N). Below the TSZ (Figure 3b), swarms and fore-mainshock sequences are more abundant in the S sector. The N and F sectors show very few clusters.

The along-strike projection of the clusters over time, above and below the TSZ, is shown in Figures 3c and 3d, respectively. Above the TSZ, clusters migrate from S toward the F sector (Figure 3c). We do not observe acceleration in foreshock sequences immediately before the 24th August mainshock (Figures 3c and 3d; Figure S14

19448007, 2023, 5, Downloaded from https://agupubs.onlinelibrary.wiley.com/doi/10.1029/2022GL101838 by CochraneItalia, Wiley Online Library on [24/03/2023]. See the Terms and Conditions (https://onlinelibrary.wiley.com/terms-and-conditions) on Wiley Online Library for rules of use; OA articles are governed by the applicable Creative Commons License

10.1029/2022GL101838

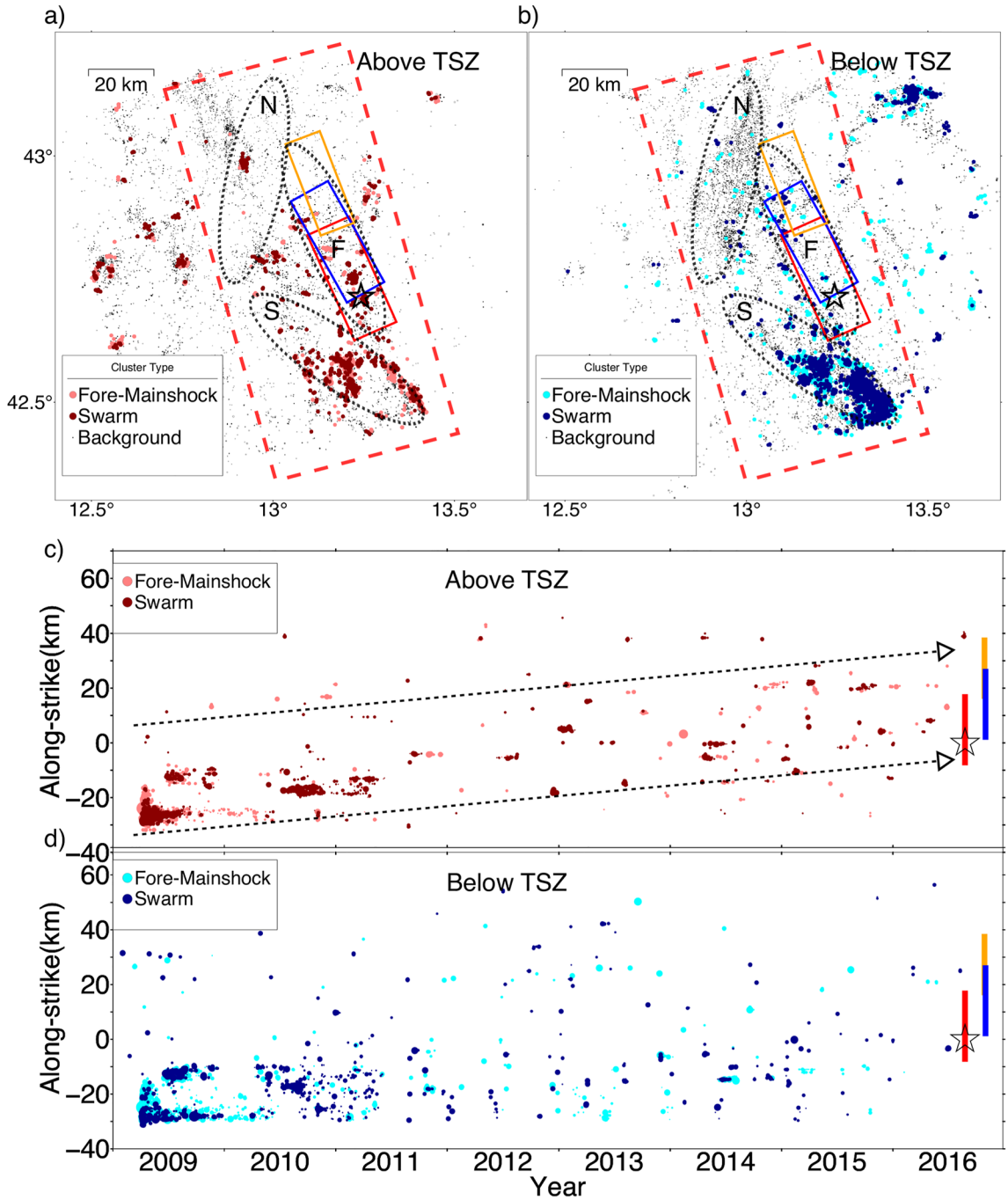

Figure 3. (a) Map showing swarm-like, foreshock-mainshock clusters and background seismicity above the TSZ, (b) as (a) below the TSZ. Only clusters with at least 10 events are shown. Dashed black lines identify the faults regions (F), the southern regions (S), where clusters prevail, and the northern region (N), where background seismicity prevails. (c) along-strike section of the clusters above the TSZ and (d) below the TSZ. Only events in the red dashed box are projected. Faults are projected for the Amatrice mainshock (red), Visso (orange), and Norcia (blue); the star marks the position of the 24th Amatrice mainshock as a reference. Only events with $M \geq$ Mc are plotted. The arrows mark the cluster migration observed in the shallower crust.

in Supporting Information S1). Clusters below the TSZ evolve differently: we find swarm-like sequences in the S sector up to 2015 (Figure 3d), while few foreshock-mainshock clusters develop within and around the F sector.

We also find repeating earthquakes, doublets characterized by low interevent time (usually less than 1 day), following a similar migration path (Figure S8 in Supporting Information S1) toward the hypocenter of the 24th August mainshock.

19448007, 2023, 5, Downloaded from https://agupubs.onlinelibrary.wiley.com/doi/10.1029/2022GL101838 by CochraneItalia, Wiley Online Library on [24/03/2023]. See the Terms and Conditions (https://onlinelibrary.wiley.com/terms-and-conditions) on Wiley Online Library for rules of use; OA articles are governed by the applicable Creative Commons License

19448007, 2023, 5, Downloaded from https://agupubs.onlinelibrary.wiley.com/doi/10.1029/2022GL101838 by CochraneItalia, Wiley Online Library on [24/03/2023]. See the Terms and Conditions (https://onlinelibrary.wiley.com/terms-and-conditions) on Wiley Online Library for rules of use; OA articles are governed by the applicable Creative Commons License

To better investigate the difference in the mechanical properties of the fault system, we use temporal clustering as a proxy for identifying areas and periods of different coupling. Generally, weaker temporal clustering characterizes creeping volumes where the coupling is lower (Liu et al., 2022). Differently, locked volumes with higher coupling show a more pronounced temporal clustering.

The coefficient of variation of interevent times (Figures 4a and 4b), the seismic moment ratio (Figures 4c and 4d), and the cumulative number of events over time (Figures 4e and 4f) are computed for the volume hosting the fault (area F in Figure 3) and for the N and S sectors of Figure 3 (Figures S15 and S16 in Supporting Information S1) to evaluate the degree of coupling above and below the TSZ.

Low and high coefficients of variation are often alternated in F. At the same time, an evident increase in temporal clustering was found in 2013 when the activity above the TSZ changed from Poissonian to clustered (Figure 4a), while below the TSZ (Figure 4b), unclustered distributed seismicity prevails.

The moment ratio is generally low after the beginning of 2013 (Figures 4c and 4d), indicating clustered swarm-like sequences, often observed elsewhere during increased over-pressurized fluids in the fault volume (Zhu et al., 2020). The cumulative events are higher above the TZS than below, rising from 2013 (Figures 4e and 4f).

In the north-northwestern sector (N), the coefficient of variation above the TSZ indicates temporal clustering lower (Figure S15a in Supporting Information S1) than in the F sector (Figure 4a). Below the TSZ, seismicity appears more sparse than in F (Figure 4b), with no apparent temporal clustering and Poissonian (Figure S15b in Supporting Information S1). Moment ratios slightly increase from 2012 above TSZ (Figure S15c in Supporting Information S1). Despite the higher density of events below the TSZ than above (Figure S15d in Supporting Information S1), moment ratios are lower than 0.5, confirming distributed low-magnitude seismicity. The weaker temporal clustering suggests low coupling for N.

South of the main fault volume (Campotosto area, S in Figure 3a), a relatively low coefficient of variation value is observed above TZS up to 2011. Subsequently, the values rise for clusters starting from the second half of 2011 (Figure S16a in Supporting Information S1).

The moment ratio shows prevailing mainshock-aftershock and foreshock-mainshock sequences up to mid-2011, followed by predominant swarm-like clusters and foreshock-mainshock (Figures S16c and S16d in Supporting Information S1). The high cumulative number of events that characterizes this sector from 2009 to mid-2011 is still related to the L'Aquila 2009 aftershock sequence (Figures S16e and S16f in Supporting Information S1).

4. Discussion

The nucleation of a dynamic rupture is related to the variations and evolution of stress and strength in the fault system volume. The two end-member models describing such a process are the cascade-up (e.g., Ellsworth & Bulut, 2018) and the pre-slip (e.g., Tape et al., 2018). Between these models, there is also the progressive deformation localization one (Ben-Zion & Zaliapin, 2020; Kato & Ben-Zion, 2021), which supposes evolving localized deformation, leading to a primary slip zone prone to a significant dynamic rupture (e.g., Amitrano et al., 1999; Renard et al., 2019).

In the pre-slip model, foreshocks are the product of an underlying quasi-stable slip process occurring around the nucleation patch. In contrast, in the cascade model, foreshocks are the engine triggering the subsequent dynamic rupture of the large earthquake (e.g., Mignan, 2014). Differently, in the progressive localization model, a more regional shear localization process induces the generation of clusters (e.g., foreshocks) along diverse minor faults surrounding the rupture zone, leading to a large earthquake (Ben-Zion & Zaliapin, 2020). In this context, monitoring microseismic activity could be crucial for tracking the evolving localization process leading to the nucleation of the mainshock rupture (Kato & Ben-Zion, 2021).

The 8-year seismicity patterns we observe show analogs with the progressive localization model proposed by Kato and Ben-Zion (2021). Before the 2016 central Italy sequence, we observe seismicity around a future rupture zone in terms of seismicity localization and coalescence of events into growing clusters in the final ∼4 years before the large earthquakes of the sequence, possibly producing crustal weakening on a multi-annual scale.

The newly retrieved catalog shows seismicity mainly occurring along a SZ (Figures 1b–1d) located below ∼7 km and bounding at depth the system of normal faults (Figure 2c, Movies S2 and S3). We observe a lower activity

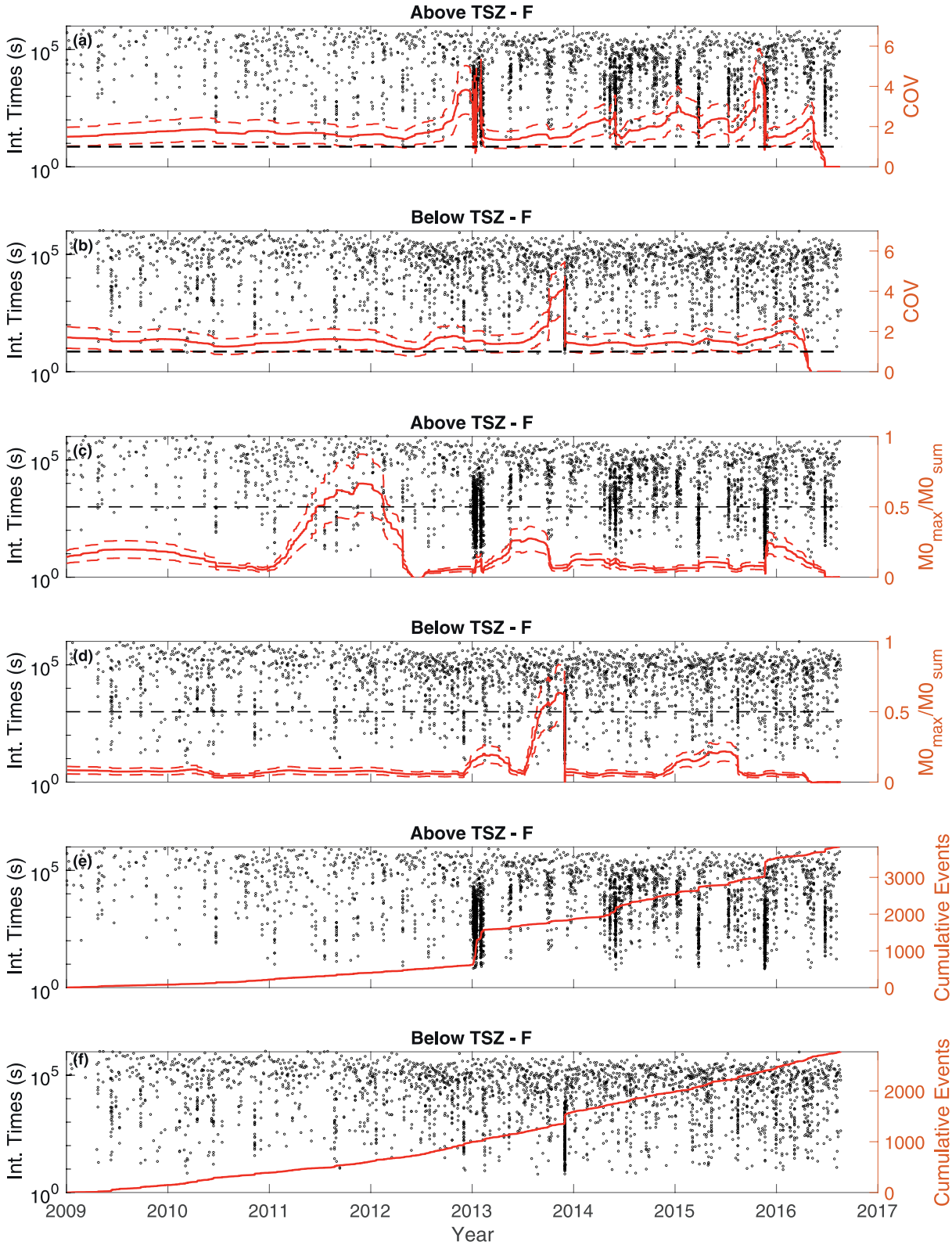

Figure 4. Coefficient of variation (COV) values of interevent times above (a) and below (b) the TSZ. Moment ratio (M0) of interevent times above (c) and below (d) the TSZ. Dashed lines show the associated standard deviation. The cumulative number of events above (e) and below (f) the TSZ is also shown. The analysis is performed for the fault volume (F in Figures 3a and 3b). Only events with $M \geq$ Mc are plotted.

19448007, 2023, 5, Downloaded from https://agupubs.onlinelibrary.wiley.com/doi/10.1029/2022GL101838 by CochraneItalia, Wiley Online Library on [24/03/2023]. See the Terms and Conditions (https://onlinelibrary.wiley.com/terms-and-conditions) on Wiley Online Library for rules of use; OA articles are governed by the applicable Creative Commons License

19448007, 2023, 5, Downloaded from https://agupubs.onlinelibrary.wiley.com/doi/10.1029/2022GL101838 by CochraneItalia, Wiley Online Library on [24/03/2023]. See the Terms and Conditions (https://onlinelibrary.wiley.com/terms-and-conditions) on Wiley Online Library for rules of use; OA articles are governed by the applicable Creative Commons License

rate along the SZ, right below the Amatrice fault (Figure 2d). While seismicity above the TSZ is organized in clusters, mainly foreshocks-mainshock and swarms, nucleating around the main fault zone (Figures 2a, 2b, and 3c), toward the Amatrice fault zone (Figures 2b and 3c, Movies S1–S3).

Above the SZ, it looks like the events migrate (Figures 2a and 2b) from the Campotosto area to the Amatrice epicenter and localize, from the end of 2012, in a 20–25 km along-strike sector. The migration observed at shallow depth from the southern portion to the fault volume (Figure 3c) and confirmed in the pattern of repeating earthquakes (Figure S8 in Supporting Information S1) suggest evidence of fluids and an aseismic slip process in this preparatory phase. Similarly, Vičič et al. (2020), using GPS data preceding the mainshock, suggest that aseismic deformation plays a fundamental role in loading surface faults of the 2016 sequence.

Observations of aseismic transients in the shallow continental crust are less common than in subduction zones (e.g., Kato et al., 2012, 2016; Uchida et al., 2016), and in areas characterized by low strain rate values such as the Apennines (Gualandi et al., 2017). It is hypothesized that slow slip requires a rich content of over-pressurized fluids and higher temperatures, components that are not often found in the colder, drier continental crust (Bouchon et al., 2013). Over-pressurized fluids (CO_2) are instead well documented along this sector of the Apennines (Chiodini et al., 2013; Lombardi et al., 2010; Trippetta et al., 2013); thus, fluid-driven slow slip can be possible in the extensional framework showing clustered activity with the presence of swarm and foreshocks. Malagnini et al. (2022) and Chiarabba et al. (2020) interpreted the 2016 Central Italy sequence as an extended episode of fluid diffusion occurring within a crust with abundant fluids. Thus, the final preparation phase leading to large earthquakes could be driven by a mixture of slow-slip transients and fluids where tiny seismic transients, testified by the presence of migrating swarm-like clusters, can contribute to the build-up of shear stress around mainshock hypocenter sites and stress changes induced by foreshock ruptures (Kato & Ben-Zion, 2021).

In 2013 within the fault volume (Figures 3 and 4a), we observed an intermittent, step-like fault slip behavior with typical swam-like clusters. This intermittent slip could represent a combination of slow and fast failure modes, increasing the stress on the eventual rupture zone and producing local variations in loading rates that modify the effective frictional behavior of the main fault.

Assuming the temporal clustering as a proxy of the main fault volume coupling, we identify the existence of a creeping activity along a basal detachment characterized by low coupling (Figure 4b), increasing the loading on the above locked high-angle normal faults (higher coupling from 2013, Figure 4a). We highlight a northwestern creeping region, where unclustered distributed seismicity prevails below the TZS (Figure S15b in Supporting Information S1), and a southern region with moderate coupling below TSZ (Figure S16b in Supporting Information S1), where fluid diffusion occurs (Figure S12 in Supporting Information S1). The low number of small magnitude events found 1 month before the mainshock and immediately before it (Figure S14 in Supporting Information S1) seems not to support the cascade or pre-slip models. At the same time, the 8-year seismicity patterns find more similarities with the progressive localization model.

5. Conclusions

The novel and increased catalog we generated, composed of about 114,000 events, highlights a progressive localization of seismicity before the first M_w 6.0 mainshock of the 2016 Central Italy sequence.

Our 8-year observations show seismic activity involving structures surrounding the nucleation and main rupture zone. The pre-sequence seismicity patterns along the almost horizontal SZ probably triggered clusters and seismicity within the main fault volume. Localization of seismicity and growing clusters migrating within the main fault volume produce crustal weakening around the future rupture zone, with progressive unlocking of surrounding zones and loading the main fault.

Migrating clusters, mainly formed by foreshocks-mainshocks and swarm-like clusters, also including repeating earthquakes, advocate the occurrence of slow slip transients, probably boosted by fluids.

Data Availability Statement

Seismic waveforms and station metadata (see STATION_LIST in Supporting Information S1) (from 1st January 2009 to 24th August 2016) used in this article are available via EIDA (the European Integrated Data Archive infrastructure within ORFEUS) at http://www.orfeus-eu.org/webdc3/. The seismic catalog presented in this study is deposited in Zenodo Open Access repository, https://doi.org/10.5281/zenodo.7515062.

Acknowledgments
This study was supported by the Real-time earthquake rIsk reduction for a reSilient Europe (RISE) project, funded by the European Union's Horizon 2020 research and innovation program under Grant Agreement Number 821115 and partially funded by the National Institute of Oceanography and Applied Geophysics (OGS). Maddalena Michele received financial support from RISE. OGS and Consorzio INteruniversitario pEr il Calcolo Automatico dell'Italia Nord Orientale (CINECA) also supported the research reported in this work under the HPC-TRES program award number 2021-01. Figures were produced using the Generic Mapping Tools (Wessel & Luis, 2017) version 6.3.0 (http://gmt.soest.hawaii.edu). We thank Ilya Zaliapin for kindly providing the declustering code. We also thank the editor Dr. Germán Prieto, David Schaff and two anonymous reviewers for helpful suggestions and constructive comments, which greatly improved this manuscript.

References

Amini, M., & Roozbeh, M. (2015). Optimal partial ridge estimation in restricted semiparametric regression models. *Journal of Multivariate Analysis*, *136*, 26–40. https://doi.org/10.1016/j.jmva.2015.01.005

Amitrano, D., Grasso, J.-R., & Hantz, D. (1999). From diffuse to localized damage through elastic interaction. *Geophysical Research Letters*, *26*(14), 2109–2112. https://doi.org/10.1029/1999gl900388

Barchi, M. R., Carboni, F., Michele, M., Ercoli, M., Giorgetti, C., Porreca, M., et al. (2021). The influence of subsurface geology on the distribution of earthquakes during the 2016–2017 Central Italy seismic sequence. *Tectonophysics*, *807*, 228797. https://doi.org/10.1016/j.tecto.2021.228797

Ben-Zion, Y., & Zaliapin, I. (2020). Localization and coalescence of seismicity before large earthquakes. *Geophysical Journal International*, *223*(1), 561–583. https://doi.org/10.1093/gji/ggaa315

Bouchon, M., Durand, V., Marsan, D., Karabulut, H., & Schmittbuhl, J. (2013). The long precursory phase of most large interplate earthquakes. *Nature Geoscience*, *6*(4), 299–302. https://doi.org/10.1038/ngeo1770

Cabrera, L., Poli, P., & Frank, W. B. (2022). Tracking the spatio-temporal evolution of foreshocks preceding the M_w 6.1 2009 L'Aquila earthquake. *Journal of Geophysical Research: Solid Earth*, *127*(3), e2021JB023888. https://doi.org/10.1029/2021JB023888

Chiarabba, C., De Gori, P., Segou, M., & Cattaneo, M. (2020). Seismic velocity pre-cursors to the 2016 M_w 6.5 Norcia (Italy) earthquake. *Geology*, *48*(9), 924–928. https://doi.org/10.1130/G47048.1

Chiaraluce, L., Di Stefano, R., Tinti, E., Scognamiglio, L., Michele, M., Casarotti, E., et al. (2017). The 2016 central Italy seismic sequence: A first look at the mainshocks, aftershocks, and source models. *Seismological Research Letters*, *88*(3), 757–771. https://doi.org/10.1785/0220160221

Chiodini, G., Cardellini, C., Caliro, S., Chiarabba, C., & Frondini, F. (2013). Advective heat transport associated with regional Earth degassing in central Apennine (Italy). *Earth and Planetary Science Letters*, *373*, 65–74. https://doi.org/10.1016/j.epsl.2013.04.009

Ellsworth, W. L., & Bulut, F. (2018). Nucleation of the 1999 Izmit earthquake by a triggered cascade of foreshocks. *Nature Geoscience*, *11*(7), 531–535. https://doi.org/10.1038/s41561-018-0145-1

Gibbons, S. J., & Ringdal, F. (2006). The detection of low magnitude seismic events using array-based waveform correlation. *Geophysical Journal International*, *165*(1), 149–166. https://doi.org/10.1111/j.1365-246X.2006.02865.x

Gualandi, A., Nichele, C., Serpelloni, E., Chiaraluce, L., Anderlini, L., Latorre, D., et al. (2017). Aseismic deformation associated with an earthquake swarm in the northern Apennines (Italy). *Geophysical Research Letters*, *44*(15), 7706–7714. https://doi.org/10.1002/2017GL073687

ISIDe Working Group. (2007). *Italian seismological instrumental and parametric database (ISIDe)*. Istituto Nazionale di Geofisica e Vulcanologia (INGV). https://doi.org/10.13127/ISIDE

Kagan, Y. Y., & Jackson, D. D. (1991). Long-term earthquake clustering. *Geophysical Journal International*, *104*(1), 117–133. https://doi.org/10.1111/j.1365-246x.1991.tb02498.x

Kato, A., & Ben-Zion, Y. (2021). The generation of large earthquakes. *Nature Reviews Earth & Environmen*t, 2(1), 26–39. https://doi.org/10.1038/s43017-020-00108-w

Kato, A., Fukuda, J., Kumazawa, T., & Nakagawa, S. (2016). Accelerated nucleation of the 2014 Iquique, Chile M_w 8.2 earthquake. *Scientific Reports*, *6*(1), 24792. https://doi.org/10.1038/srep24792

Kato, A., Obara, K., Igarashi, T., Tsuruoka, H., Nakagawa, S., & Hirata, N. (2012). Propagation of slow slip leading up to the 2011 M_w 9.0 Tohoku-Oki earthquake. *Science*, *335*(2), 705–708. https://doi.org/10.1126/science.1215141

Liu, Y.-K., Ross, Z. E., Cochran, E. S., & Lapusta, N. (2022). A unified perspective of seismicity and fault coupling along the San Andreas Fault. *Science Advances*, *8*, eabk1167. https://doi.org/10.1126/sciadv.abk1167

Lomax, A., Virieux, J., Volant, P., & Berge, C. (2000). Probabilistic earthquake location in 3D and layered models: Introduction of a metropolis-Gibbs method and comparison with linear locations. In C. H. Thurber & N. Rabinowitz (Eds.), *Advances in seismic event location* (pp. 101–134). Kluwer.

Lombardi, A. M., Cocco, M., & Marzocchi, W. (2010). On the increase of background seismicity rate during the 1997–1998 Umbria-Marche, central Italy, sequence: Apparent variation or fluid-driven triggering? *Bulletin of the Seismological Society of America*, *100*(3), 1138–1152. https://doi.org/10.1785/0120090077

Lucente, F. P., De Gori, P., Margheriti, L., Piccinini, D., Di Bona, M., Chiarabba, C., & Piana Agostinetti, N. (2010). Temporal variation of seismic velocity and anisotropy before the 2009 M_w 6.3 L'Aquila earthquake, Italy. *Geology*, *38*(11), 1015–1018. https://doi.org/10.1130/G31463.1

Malagnini, L., Lucente, F. P., De Gori, P., Akinci, A., & Munafò, I. (2012). Control of pore fluid pressure diffusion on fault failure mode: Insights from the 2009 L'Aquila seismic sequence. *Journal of Geophysical Research*, *117*(B5), B05302. https://doi.org/10.1029/2011JB008911

Malagnini, L., Parsons, T., Munafò, I., Mancini, S., Segou, M., & Geist, E. L. (2022). Crustal permeability changes inferred from seismic attenuation: Impacts on multi-mainshock sequences. *Frontiers of Earth Science*, *10*, 963689. https://doi.org/10.3389/feart.2022.963689

Mandler, E., Pintori, F., Gualandi, A., Anderlini, L., Serpelloni, E., & Belardinelli, M. E. (2021). Post-seismic deformation related to the 2016 Central Italy seismic sequence from GPS displacement time-series. *Journal of Geophysical Research*, *126*(9), e2021JB022200. https://doi.org/10.1029/2021JB022200

Mignan, A. (2014). The debate on the prognostic value of earthquake foreshocks: A meta-analysis. *Scientific Reports*, *4*(1), 4099. https://doi.org/10.1038/srep04099

Ogata, Y., & Katsura, K. (2012). Prospective foreshock forecast experiment during the last 17 years. *Geophysical Journal International*, *191*, 1237–1244. https://doi.org/10.1111/j.1365-246X.2012.05645.x

Renard, F., McBeck, J., Kandula, N., Cordonnier, B., Meakin, P., & Ben-Zion, Y. (2019). Volumetric and shear processes in crystalline rock approaching faulting. *Proceedings of the National Academy of Sciences of the United States of America*, *116*(33), 16234–16239. https://doi.org/10.1073/pnas.1902994116

Ripepe, M., Piccinini, D., & Chiaraluce, L. (2000). Foreshock sequence of September 26th, 1997 Umbria-Marche earthquakes. *Journal of Seismology*, *4*(4), 387–399. https://doi.org/10.1023/a:1026508425230

Scognamiglio, L., Tinti, E., Casarotti, E., Pucci, S., Villani, F., Cocco, M., et al. (2018). Complex fault geometry and rupture dynamics of the M_w 6.5, 30 October 2016, Central Italy earthquake. *Journal of Geophysical Research: Solid Earth*, *123*(4), 2943–2964. https://doi.org/10.1002/2018JB015603

Scognamiglio, L., Tinti, E., & Quintiliani, M. (2006). Time domain moment Tensor (TDMT) [Dataset]. Istituto Nazionale di Geofisica e Vulcanologia (INGV). https://doi.org/10.13127/TDMT

Sugan, M., Campanella, S., Vuan, A., & Shakibay Senobari, N. (2022). A Python code for detecting true repeating earthquakes from Self-similar waveforms (FINDRES). *Seismological Research Letters*, *93*(5), 2847–2857. https://doi.org/10.1785/0220220048

Sugan, M., Kato, A., Miyake, H., Nakagawa, S., & Vuan, A. (2014). The preparatory phase of the 2009 M_w 6.3 L'Aquila earthquake by improving the detection capability of low-magnitude foreshocks. *Geophysical Research Letters*, *41*(17), 6137–6144. https://doi.org/10.1002/2014GL061199

19448007, 2023, 5, Downloaded from https://agupubs.onlinelibrary.wiley.com/doi/10.1029/2022GL101838 by CochraneItalia, Wiley Online Library on [24/03/2023]. See the Terms and Conditions (https://onlinelibrary.wiley.com/terms-and-conditions) on Wiley Online Library for rules of use; OA articles are governed by the applicable Creative Commons License

Sugan, M., Vuan, A., Kato, A., Massa, M., & Amati, G. (2019). Seismic evidence of an early afterslip during the 2012 sequence in Emilia (Italy). *Geophysical Research Letters*, *46*(2), 625–635. https://doi.org/10.1029/2018GL079617

Tan, Y. J., Waldhauser, F., Ellsworth, W. L., Zhang, M., Zhu, W., Michele, M., et al. (2021). Machine-learning-based high-resolution earthquake catalog reveals how complex fault structures were activated during the 2016–2017 Central Italy sequence. *The Seismic Record*, *1*, 11–19. https://doi.org/10.1785/0320210001

Tape, C., Holtkamp, S., Silwal, V., Hawthorne, J., Kaneko, Y., Ampuero, J. P., et al. (2018). Earthquake nucleation and fault slip complexity in the lower crust of central Alaska. *Nature Geoscience*, *11*(7), 536–541. https://doi.org/10.1038/s41561-018-0144-2

Tinti, E., Scognamiglio, L., Michelini, A., & Cocco, M. (2016). Slip heterogeneity and directivity of the ML 6.0, 2016, Amatrice earthquake estimated with rapid finite-fault inversion. *Geophysical Research Letters*, *43*(20), 10745–10752. https://doi.org/10.1002/2016GL071263

Trippetta, F., Collettini, C., Barchi, M. R., Lupattelli, A., & Mirabella, F. (2013). A multidisciplinary study of a natural example of a CO_2 geological reservoir in Central Italy. *International Journal of Greenhouse Gas Control*, *12*, 72–83. https://doi.org/10.1016/j.ijggc.2012.11.010

Uchida, N. (2019). Detection of repeating earthquakes and their application in characterizing slow fault slip. *Progress in Earth and Planetary Science*, *6*(1), 40. https://doi.org/10.1186/s40645-019-0284-z

Uchida, N., Iinuma, T., Nadeau, R. M., Bürgmann, R., & Hino, R. (2016). Periodic slow slip triggers megathrust zone earthquakes in northeastern Japan. *Science*, *351*(6272), 488–492. https://doi.org/10.1126/science.aad3108

Valoroso, L., Chiaraluce, L., Piccinini, D., Di Stefano, R., Schaff, D., & Waldhauser, F. (2013). Radiography of a normal fault system by 64,000 high-precision earthquake locations: The 2009 L'Aquila (Central Italy) case study. *Journal of Geophysical Research*, *118*(3), 1156–1176. https://doi.org/10.1002/jgrb.50130

Vičič, B., Aoudia, A., Borghi, A., Momeni, S., & Vuan, A. (2020). Seismicity rate changes and geodetic transients in Central Apennines. *Geophysical Research Letters*, *47*(22), e2020GL090668. https://doi.org/10.1029/2020GL090668

Vuan, A., Brondi, P., Sugan, M., Chiaraluce, L., Di Stefano, R., & Michele, M. (2020). Intermittent slip along the Alto Tiberina low-angle normal fault in Central Italy. *Geophysical Research Letters*, *47*(17), e2020GL089039. https://doi.org/10.1029/2020GL089039

Vuan, A., Sugan, M., Amati, G., & Kato, A. (2018). Improving the detection of low-magnitude seismicity preceding the M_w 6.3 L'Aquila earthquake: Development of a scalable code based on the cross-correlation of template earthquakes. *Bulletin of the Seismological Society of America*, *108*(1), 471–480. https://doi.org/10.1785/0120170106

Vuan, A., Sugan, M., Chiaraluce, L., & Di Stefano, R. (2017). Loading rate variations along a mid-crustal shear zone preceding the M_w 6.0 earthquake of 24 August 2016 in Central Italy. *Geophysical Research Letters*, *44*. https://doi.org/10.1002/2017GL076223

Waldhauser, F., & Ellsworth, W. L. (2000). A double-difference earthquake location algorithm: Method and application to the northern Hayward Fault, California. *Bulletin of the Seismological Society of America*, *90*(6), 1353–1368. https://doi.org/10.1785/0120000006

Waldhauser, F., Michele, M., Chiaraluce, L., Di Stefano, R., & Schaff, D. P. (2021). Fault planes, fault zone structure and detachment fragmentation resolved with high precision aftershock locations of the 2016–2017 Central Italy sequence. *Geophysical Research Letters*, *48*(16), e2021GL092918. https://doi.org/10.1029/2021GL092918

Wessel, P., & Luis, J. F. (2017). The GMT/MATLAB toolbox. *Geochemistry, Geophysics, Geosystems*, *18*(2), 811–823. https://doi.org/10.1002/2016GC006723

Zaliapin, I., & Ben-Zion, Y. (2016). A global classification and characterization of earthquake clusters. *Geophysical Journal International*, *207*(1), 608–634. https://doi.org/10.1093/gji/ggw300

Zaliapin, I., & Ben-Zion, Y. (2020). Earthquake declustering using the nearest-neighbor approach in the space-time-magnitude domain. *Journal of Geophysical Research*, *125*, e2018JB017120. https://doi.org/10.1029/2018JB017120

Zhu, W., Allison, K. L., Dunham, E. M., & Yang, Y. (2020). Fault valving and pore pressure evolution in simulations of earthquake sequences and aseismic slip. *Nature Communications*, *11*(1), 4833. https://doi.org/10.1038/s41467-020-18598-z

References From the Supporting Information

Baillard, C., Crawford, W. C., Ballu, V., Hibert, C., & Mangeney, A. (2014). An automatic Kurtosis-based P- and S-phase picker designed for local seismic networks. *Bulletin of the Seismological Society of America*, *104*(1), 394–409. https://doi.org/10.1785/0120120347

Cao, A. M., & Gao, S. S. (2002). Temporal variations of seismic b-values beneath northeastern Japan island arc. *Geophysical Research Letters*, *29*(9), 48-1–48-3. https://doi.org/10.1029/2001GL013775

Carannante, S., Monachesi, G., Cattaneo, M., Amato, A., & Chiarabba, C. (2013). Deep structure and tectonics of the northern-central Apennines as seen by regional-scale tomography and 3-D located earthquakes. *Journal of Geophysical Research*, *118*(10), 5391–5403. https://doi.org/10.1002/jgrb.50371

Chen, K. H., Nadeau, R. M., & Rau, R.-J. (2008). Characteristic repeating earthquakes in an arc-continent collision boundary zone: The Chihshang fault of eastern Taiwan. *Earth and Planetary Science Letters*, *276*(3–4), 262–327. https://doi.org/10.1016/j.epsl.2008.09.021

Crotwell, H. P., Owens, T. J., & Ritsema, J. (1999). The TauP Toolkit: Flexible seismic travel-time and ray-path utilities. *Seismological Research Letters*, *70*(2), 154–160. https://doi.org/10.1785/gssrl.70.2.154

Eshelby, J. D. (1957). The determination of the elastic field of an ellipsoidal inclusion and related problems. *Proceedings of the Royal Society of London A*, *241 1226*, 376–396.

INGV Seismological Data Centre. (2006). *Rete sismica nazionale (RSN)*. Istituto Nazionale di Geofisica e Vulcanologia (INGV). https://doi.org/10.13127/SD/X0FXNH7QFY

Krischer, L., Megies, T., Barsch, R., Beyreuther, M., Lecocq, T., Caudron, C., & Wassermann, J. (2015). ObsPy: A bridge for seismology into the scientific Python ecosystem. *Computational Science & Discovery*, *8*(1), 014003. https://doi.org/10.1088/1749-4699/8/1/014003

Michele, M., Chiaraluce, L., Di Stefano, R., & Waldhauser, F. (2020). Fine-scale structure of the 2016–2017 Central Italy seismic sequence from data recorded at the Italian National Network. *Journal of Geophysical Research: Solid Earth*, *125*(4), e2019JB018440. https://doi.org/10.1029/2019JB018440

Michele, M., Latorre, D., & Emolo, A. (2019). An empirical formula to classify the quality of earthquake locations. *Bulletin of the Seismological Society of America*, *109*(6), 2755–2761. https://doi.org/10.1785/0120190144

Munafò, I., Malagnini, L., & Chiaraluce, L. (2016). On the relationship between M_w and M_L for small earthquakes. *Bulletin of the Seismological Society of America*, *106*(5), 2402–2408. https://doi.org/10.1785/0120160130

Peng, Z., & Zhao, P. (2009). Migration of early aftershocks following the 2004 Parkfield earthquake. *Nature Geoscience*, 2(12), 877–881. https://doi.org/10.1038/ngeo697

19448007, 2023, 5, Downloaded from https://agupubs.onlinelibrary.wiley.com/doi/10.1029/2022GL101838 by CochraneItalia, Wiley Online Library on [24/03/2023]. See the Terms and Conditions (https://onlinelibrary.wiley.com/terms-and-conditions) on Wiley Online Library for rules of use; OA articles are governed by the applicable Creative Commons License

Poupinet, G., Ellsworth, W. L., & Frechet, J. (1984). Monitoring velocity variations in the crust using earthquake doublets: An application to California's Calaveras fault. *Journal of Geophysical Research*, *89*(B7), 5719–5731. https://doi.org/10.1029/jb089ib07p05719

Ross, Z. E., Trugman, D. T., Hauksson, E., & Shearer, P. M. (2019). Searching for hidden earthquakes in Southern California. *Science*, *364*(6442), 767–771. https://doi.org/10.1126/science.aaw6888

Simon, V., Kraft, T., Diehl, T., & Tormann, T. (2021). Possible precursory slow-slip to two ML∼3 main events of the Diemtigen microearthquake sequence, Switzerland. *Geophysical Research Letters*, *48*(19), e2021GL093783. https://doi.org/10.1029/2021GL093783

Wiemer, S., & Wyss, M. (2000). Minimum magnitude of complete reporting in earthquake catalogs: Examples from Alaska, the western United States, and Japan. *Bulletin of the Seismological Society of America*, *90*(4), 859–869. https://doi.org/10.1785/0119990114

19448007, 2023, 5, Downloaded from https://agupubs.onlinelibrary.wiley.com/doi/10.1029/2022GL101838 by CochraneItalia, Wiley Online Library on [24/03/2023]. See the Terms and Conditions (https://onlinelibrary.wiley.com/terms-and-conditions) on Wiley Online Library for rules of use; OA articles are governed by the applicable Creative Commons License